Supplementary Information

Shape-dependent Internalization Kinetics of Nanoparticle by Membrane

Liping Chen,† Shiyan Xiao∗,† Hong Zhu,† Lei Wang,† and Haojun Liang,‡,¶

CAS Key Laboratory of Soft Matter Chemistry, Department of Polymer Science and Engineering, University of Science and Technology of China, Hefei, Anhui 230026, P. R. China., CAS Key Laboratory of Soft Matter Chemistry, Collaborative Innovation Center of Chemistry for Energy Materials, Department of Polymer Science and Engineering, University of Science and Technology of China, Hefei, Anhui 230026, P. R. China., and Hefei National Laboratory for Physical Sciences at Microscale, University of Science and Technology of China, Hefei, Anhui, 230026, P. R. China.
E-mail: xiaosy@ustc.edu.cn
Phone: +86 (0)551 63607701. Fax: +86 (0)551 63607824

∗To whom correspondence should be addressed
†CAS Key Laboratory of Soft Matter Chemistry
‡CAS Key Laboratory of Soft Matter Chemistry, Collaborative Innovation Center of Chemistry for Energy Materials
¶Hefei National Laboratory for Physical Sciences at Microscale

Definition of Angle

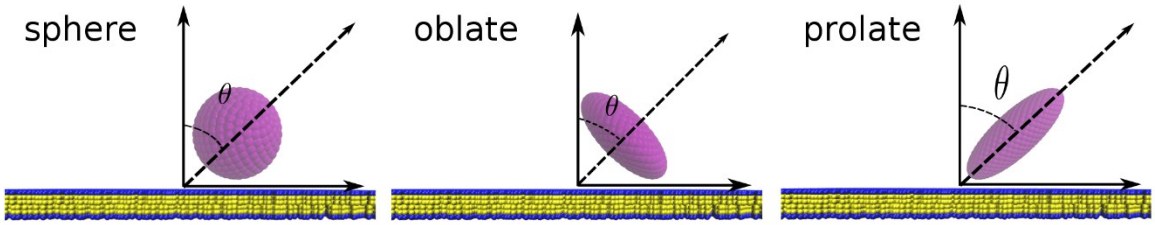

Figure S1: The definition of changing angle for different nanoparticles. The spherical nanoparticle can be defined as $\frac{x^2+y^2}{D^2}+\frac{z^2}{L^2}=1$. The dash-lines with an arrow represent the z-axis of nanoparticle. The angle θ is the included angle between the spheroid nanoparticle's z-axis and the normal vector of membrane plane. The initial angles are not same for the three types of nanoparticles. The oblate nanoparticle's initial angle is 90 degree, and it is 0 degree for prolate nanoparticle.

Calculation of the coverage of nanoparticles

In our models, the nanoparticles are constructed using beads. If the space within a radius (1.35σ) of one bead is occupied by at least one lipid, then we define the bead is wrapped by membrane, otherwise it is not. And the coverage percentage is calculated by the ratio between the amount of wrapped beads and the total amount of beads of the particle.

Testing of particle-membrane systems with different box lengths in *x*- and *y*-dimensions

In order to study the effect of box size on the process of particle endocytosis, the particles were simulated in boxes with different lengths in *x*-/*y*-dimensions (l_x=l_y). Note that the box length in *z*-dimension (l_z) was set to 100.00σ in all simulated systems. For the particles with a volume of $288\pi\sigma^3$, three types of box length (l_x = l_y = 66.67, 100.00 and 150.00σ) have been tested. For the particles with a volume of $972\pi\sigma^3$, two types of box length (100 and 150σ) have been used for l_x and l_y. The number density of lipid in the *xy*-plane is the same for all simulated systems, that is, the amount of lipid is different for the systems with different box lengths in the *x*- and *y*-dimensions.

Time evolution profiles of the averaged coverage percentage, averaged orientation are presented in Figs. S2 and S3. It is shown that the particle uptake processes are very close for the particles having the same volume simulated using different box sizes. In addition, the endocytic times are close for the particle-membrane systems simulated using different box lengths in *x*- and *y*-dimensions (Fig. S4). It should be emphasized that this slight difference in endocytic times does not change the conclusions we presented in the main text. Based on our testing, it is proven that a simulation box with length of 100σ in *x*- and *y*-dimensions is large enough to avoid the box size effect on the kinetics of particle endocytosis, and the results presented herein are credible and convincing.

In the current work, all the results presented in the main text and Supplementary Information are derived for the systems simulated in cubic boxes of length 100σ.

Time evolution of the averaged coverage percentage for particles simulated in boxes with different sizes

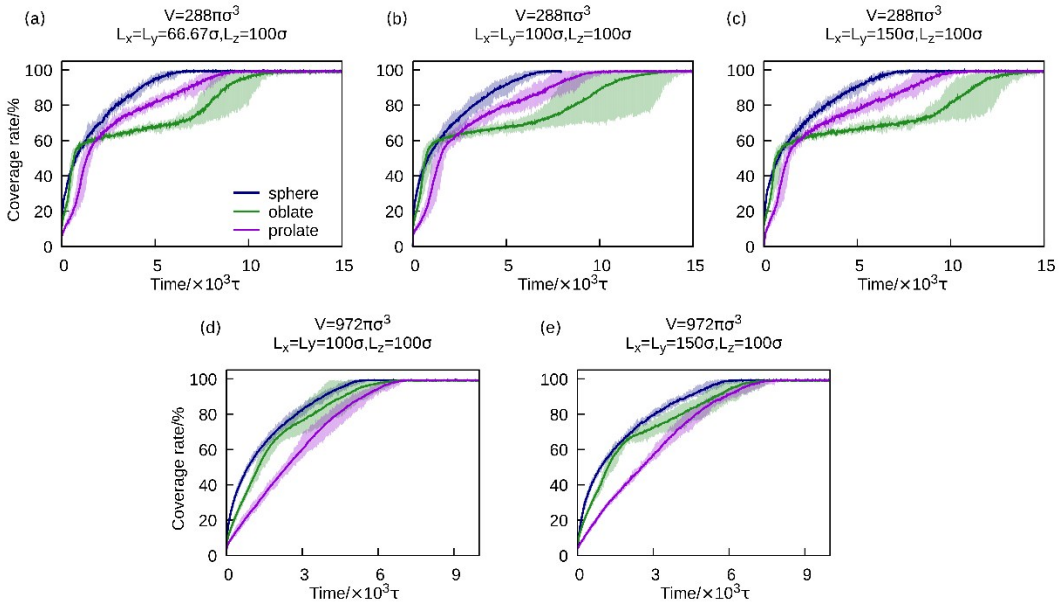

Figure S2: Time evolution of the averaged coverage percentage for the spherical, oblate (ρ = 0.4) and prolate (ρ = 3.0) nanoparticles with volumes of 288 and 972 $\pi\sigma^3$. The shading area around the average line shows the maximum and minimum range of the data. The box lengths in x- and y-dimensions (l_x and l_y) were set to 66.67 (a), 100 (b) and 150σ (c) for the particle with a volume of 288 $\pi\sigma^3$, and were set to 100 (d) and 150σ (e) for the particle with a volume of 288 $\pi\sigma^3$. The box lengths in z-dimensions (l_z) were set to 100σ in all simulated systems. The interaction strength (α) is 1.1.

Time evolution of the averaged orientation for particles simulated in boxes with different sizes

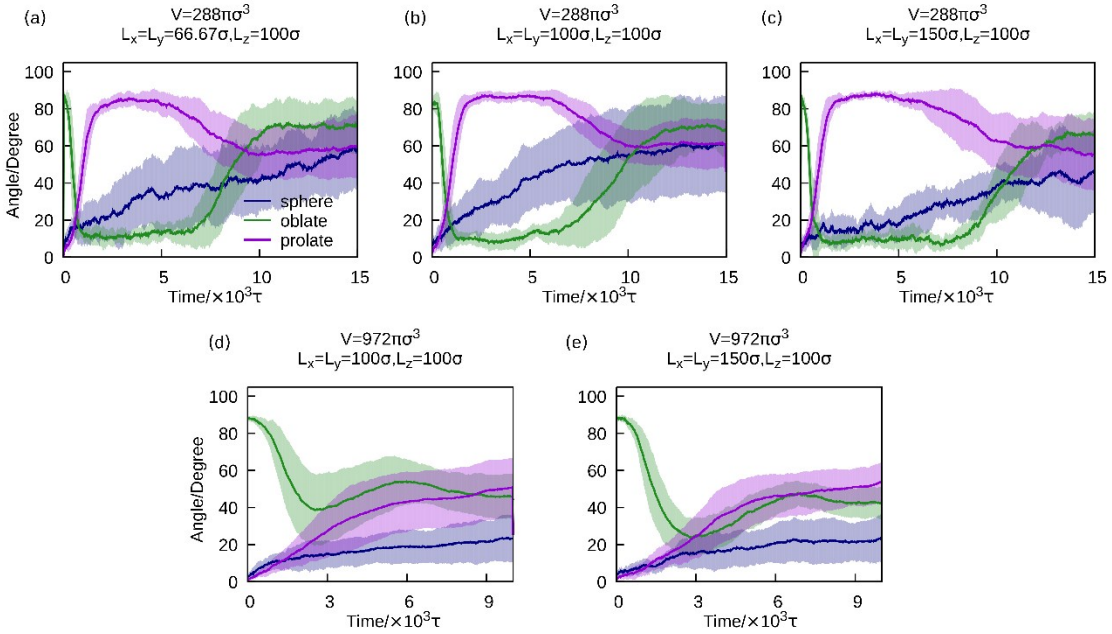

Figure S3: Time evolution of the averaged orientation for the spherical, oblate (ρ = 0.4) and prolate (ρ = 3.0) nanoparticles with volumes of 288 and 972 $\pi\sigma^3$. The shading area around the average line shows the two standard deviation range of the data. The box lengths in *x*- and *y*-dimensions were set to 66.67 (a), 100 (b) and 150σ (c) for the particle with a volume of 288 $\pi\sigma^3$, and were set to 100 (d) and 150σ (e) for the particle with a volume of 288 $\pi\sigma^3$. The box lengths in z-dimensions were set to 100σ in all simulated systems. The interaction strength (α) is 1.1.

Endocytic time for particles simulated in boxes with different sizes.

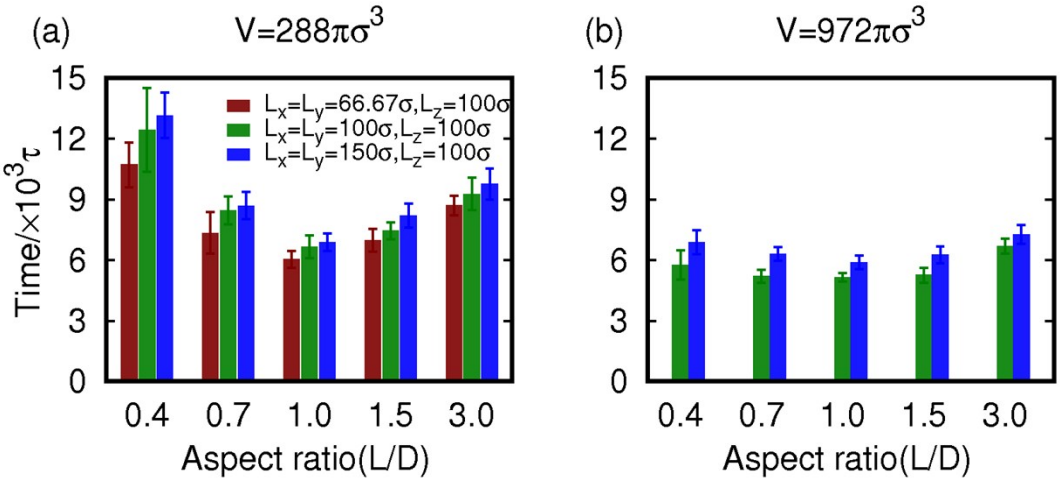

Figure S4: Endocytic time for nanoparticles simulated in boxes with different sizes. The testing were performed to the particles with volumes of 288 (a) and 972 $\pi\sigma^3$ (b).

Time evolution of nanoparticle locations along the membrane normal vector

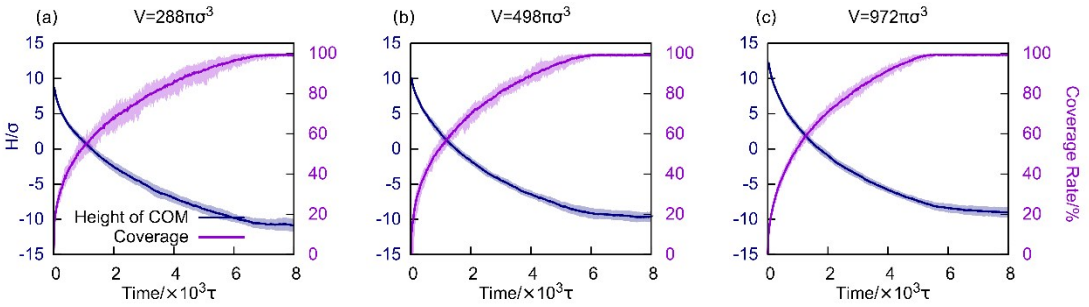

Figure S5: Time evolutions of nanoparticle locations and wrapping percentage along the membrane normal vector.

Time evolution of averaged orientation angle of spherical particles with varied volumes ($\alpha = 1.1$)

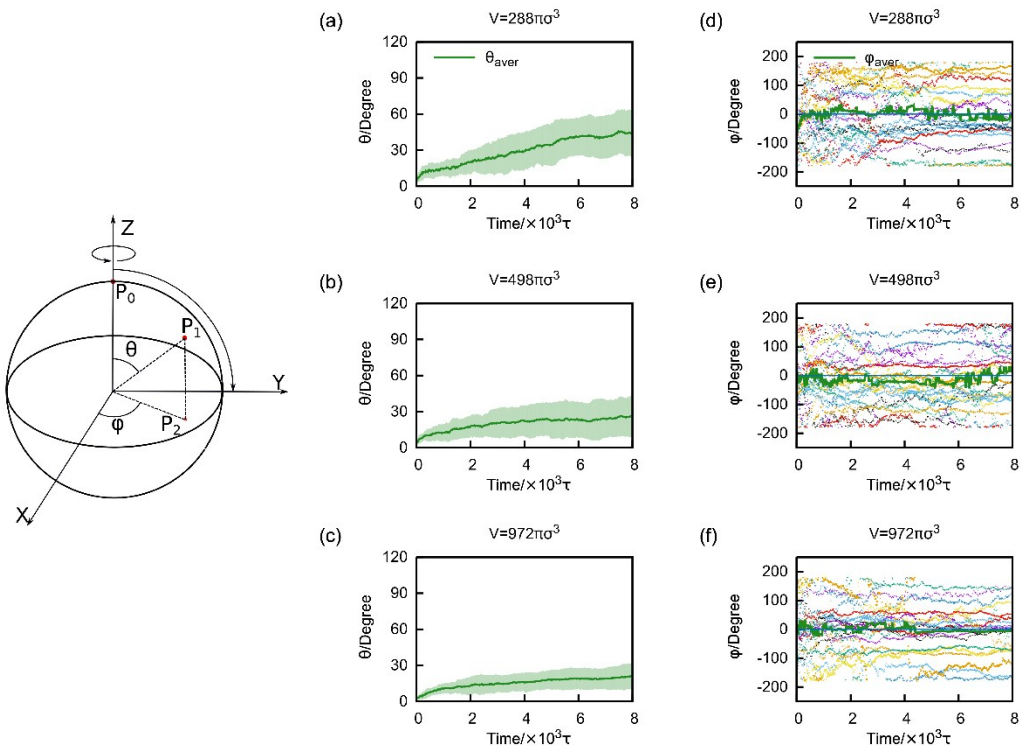

Figure S6: Time evolution of averaged orientation angle of spherical particles with varied volumes ($\alpha = 1.1$), derived from twenty independent trajectories. (a), (b) and (c) display the average angles evolve as a function of time, and the shading area around the average line shows the two standard deviation range of the data calculated at this time point among the twenty trajectories. (d), (e) and (f) display the profile of the individual trajectory for these three types of spheres, and the bold forest green line indicates the average value of φ.

Time evolution of the distance between the center of spherical particle and its position at the initial state

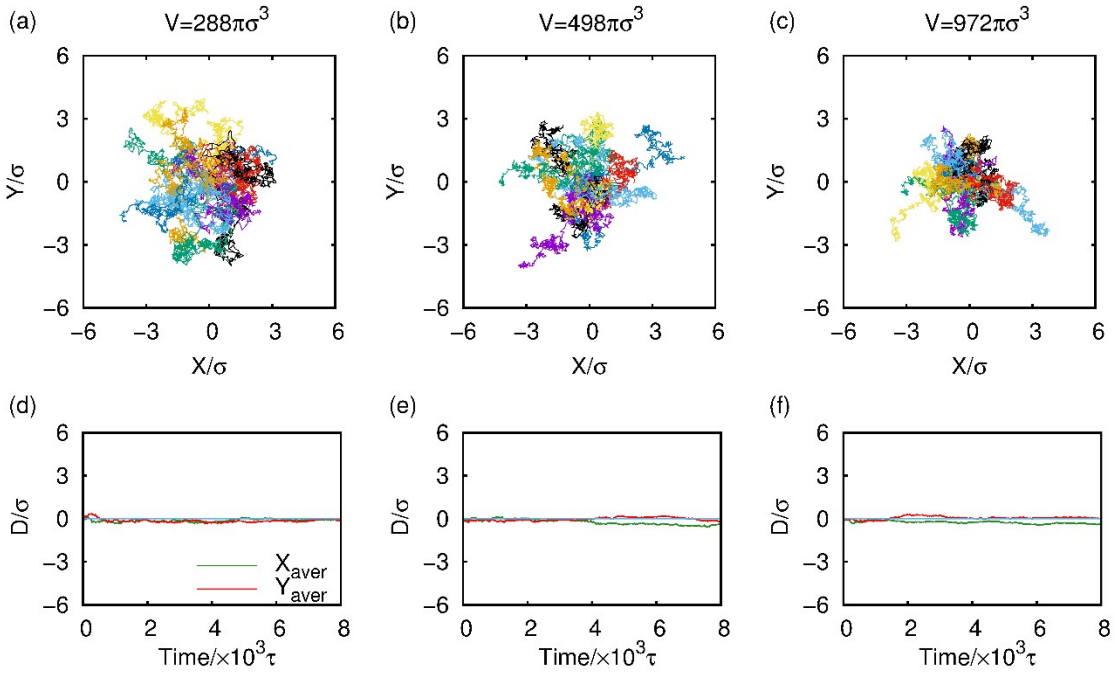

Figure S7: Time evolution of the vector from the center of spherical particle to its position at the initial state. Each profile with one kind of color represent one simulated trajectory. (a), (b), and (c) display the profiles of this vector for these simulated systems with varied volumes. (d), (e), and (f) display time evolution of the x and y components of the vector averaged using these twenty simulated trajectories for each system.

Time evolution of the orientation of particles with a volume of $972\pi\sigma^3$ ($\alpha = 1.1$) and a particle mass reduced by half, for five independent simulation trajectories

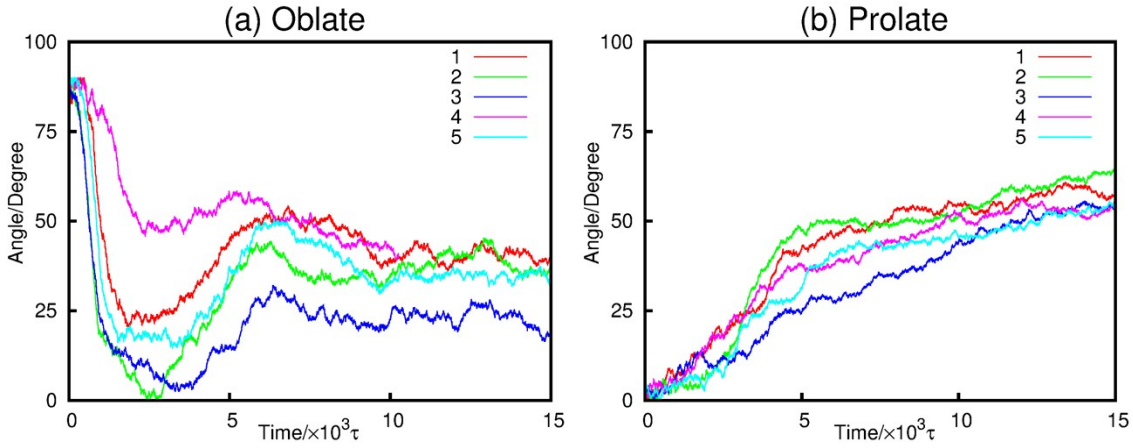

Figure S8: Time evolution of the orientation for oblate (ρ = 0.4) and prolate (ρ= 3.0) nanoparticles with a volume of $972\pi\sigma^3$ and a particle mass reduced by half. The interaction strength (α) is 1.1.

Angle between the ellipsoids and membrane midplane

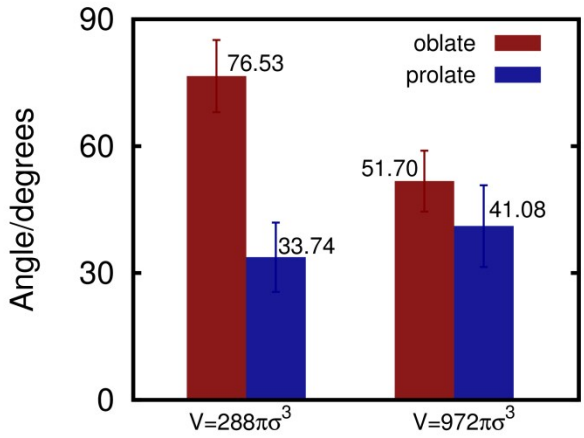

Figure S9: The entry angle between the ellipsoids (ρ = 0.4 and 3.0 for oblate and prolate particles, respectively) and membrane midplane. If we define the angle $\emptyset$ as the angel between the z axis of the prolate ellipsoid and membrane midplane, then the entry angle is $\emptyset$ and $90° - \emptyset$ for prolate and oblate particles, respectively.

The endocytic pathway of ellipsoidal particle with a volume of $288\pi\sigma^3$ ($\alpha = 1.1$)

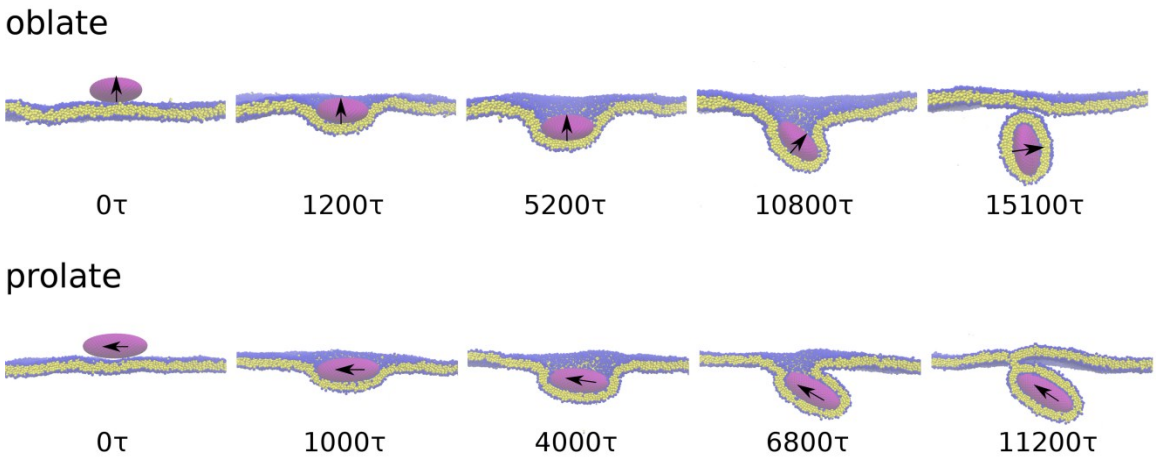

Figure S10: Representative snapshots of endocytic pathway for oblate (upper, $\rho = 0.4$) and prolate (lower, $\rho = 3.0$) nanoparticles with a volume of $288\pi\sigma^3$. A cut through the membrane at the particle position is depicted for clarity. The beads of the nanoparticle are displayed in purple. For membrane, the beads of head groups are in blue, and tail beads are in yellow. And the interaction strength (α) is set to 1.1. **At the beginning of our simulations, the particles were placed at the upper side of the membrane, with the z axis perpendicular and parallel to the membrane for oblate and prolate particles, respectively.**

The endocytic pathway of ellipsoidal particle with a volume of $972\pi\sigma^3$ ($\alpha = 1.1$)

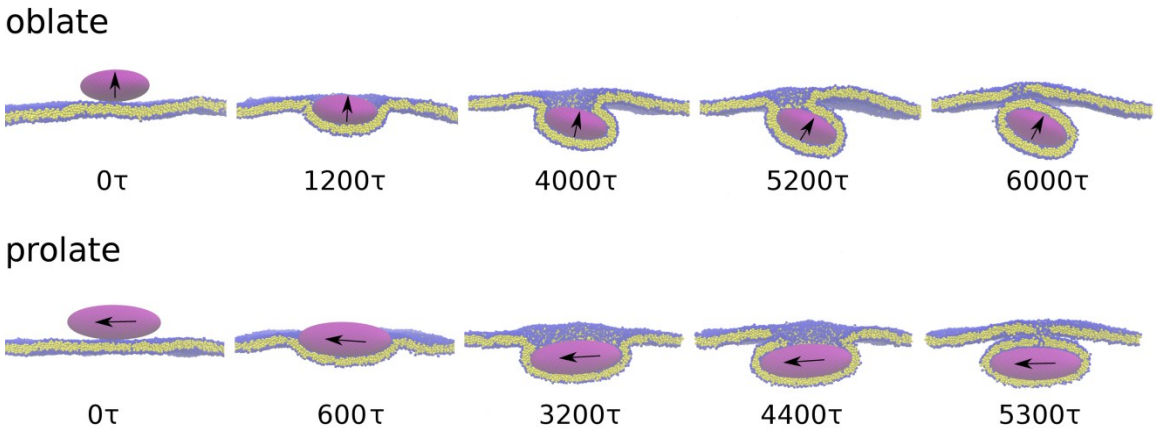

Figure S11: Representative snapshots of endocytic pathway for oblate (upper, ρ = 0.4) and prolate (lower, ρ = 3.0) nanoparticles with a volume of $972\pi\sigma^3$. A cut through the membrane at the particle position is depicted for clarity. The beads of the nanoparticle are displayed in purple. For membrane, the beads of head groups are in blue, and tail beads are in yellow. And the interaction strength (α) is set to 1.1. **At the beginning of our simulations, the particles were placed at the upper side of the membrane, with the z axis perpendicular and parallel to the membrane for oblate and prolate particles, respectively.**

Free energy calculations

To further understand the endocytic processes of nanoparticles with different shapes, thermodynamic integration (TI) approach was employed to calculate the free energy changes of the systems during particle internalization. A parameter λ defined as $z(\lambda) = z(\lambda = 0) + \lambda \cdot [z(\lambda = 1) - z(\lambda = 0)]$ was adapted to measure the normalized distance from the center of the particle to the membrane midplane in the *z*-direction. $\lambda = 0$ corresponds to the initial position of nanoparticle at one side of the membrane with the distance out of the cut-off distance of LJ potential; and λ is set to 1 when the vesicle containing the particle and the flat membrane is completely separated. For all the systems investigated in the present work, the endocytic process is divided into a series of λ values between 0 and 1. The development from state λ_i to state λ_{i+1} corresponds to movement in the *z*-direction for nanoparticle. The free energy change of endocytosis is expressed as [1]:

$$\Delta F = \int_{\lambda=0}^{\lambda} \frac{\partial F(\lambda)}{\partial \lambda} d\lambda$$

.

For each chosen value of λ with its equilibrium position at $z(\lambda)$, a harmonic potential $U(\lambda) = k_z[Z - z(\lambda)]^2/2$ is imposed to confine the motion of particle in the z-direction, where k_z is the spring constant and set to 300. The sampling simulation for each λ lasts around 1000τ (~100,000 steps), and the particle is forced to oscillate around a pseudo-equilibrium position $< Z >$ in the vicinity of $z(\lambda)$. The free energy change can be derived from the constrained interactions between the particle and its surroundings,

$$\Delta F = \int_{\lambda=0}^{\lambda} k_z[z(\lambda) - < Z >]d\lambda$$

and then rewritten as[2]: , with $0 \leq \lambda \leq 1$. The free energy calculations were performed for particles with a volume of 288 or $972\pi\sigma^3$ and α = 1.2. α is the interaction strength to regulate the interactions between the lipid "head" and nanoparticles.

[1] F. Leroy, D. J. V. A. dos Santos and F. Müller-Plathe, *Macromol. Rapid Commun.*, **2009**, 30, 864-870.
[2] Y. Li, X. Li, Z. Li and H. Gao, *Nanoscale*, **2012**, 4, 3768–3775.

Profile of potential mean force (PMF) in k_BT associated with the internalization of nanoparticle as a function of the distance between the particle center and bilayer midplane

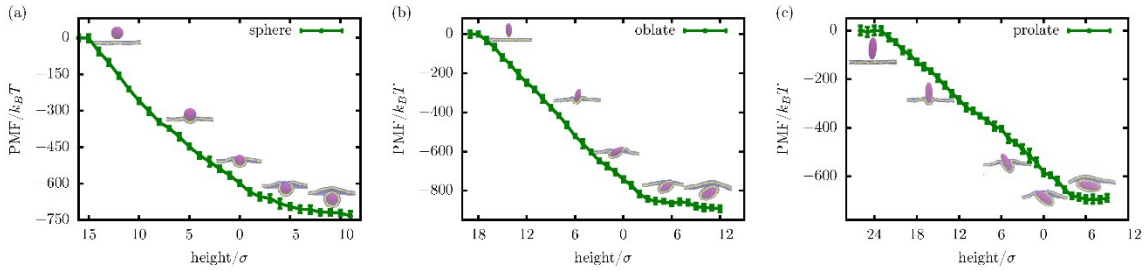

Figure S12: Profile of potential mean force (PMF) in k_BT associated with the internalization of nanoparticle as a function of the distance between the particle center and bilayer midplane. The interaction strength (α) is set to 1.2, and the volumes of particles are $972\pi\sigma^3$. The values of aspect ratio are 0.4 and 3.0 for oblate and prolate ellipsoids, respectively. The endocytic process starts from the state that the nanoparticle is located out of the interaction of the interaction cut-off from the bilayer surface.

The endocytic pathways of different type of nanoparticles ($\alpha = 1.3$).

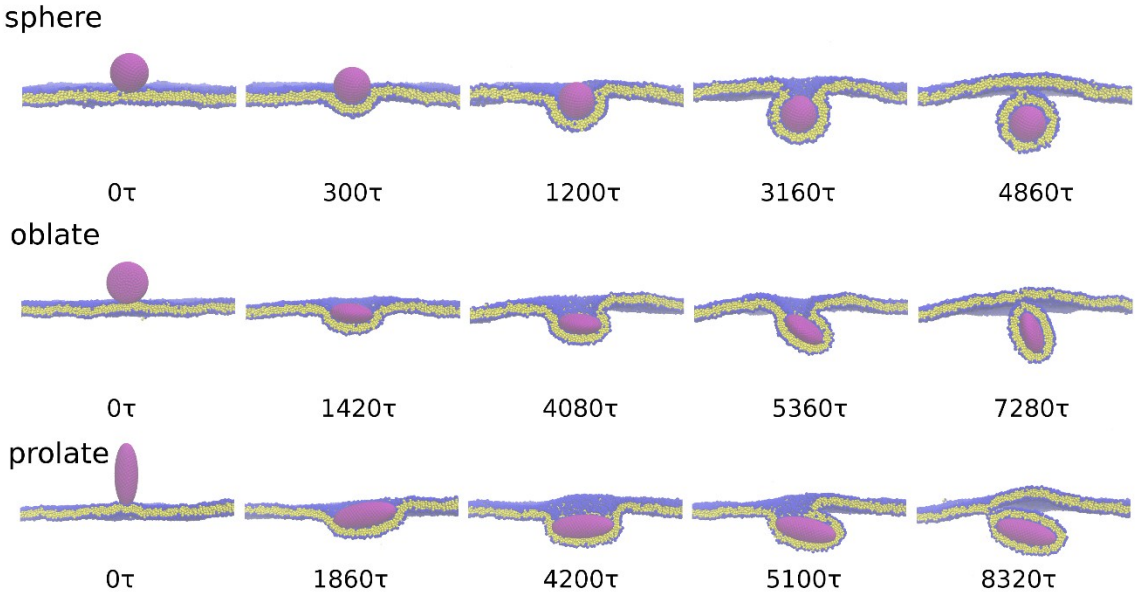

Figure S13: Representative snapshots of endocytic pathway for spherical (upper), oblate (middle, ρ = 0.4), prolate (lower, ρ = 3.0) nanoparticles with a volume of $288\pi\sigma^3$. A cut through the membrane at the particle position is depicted for clarity. The beads of the nanoparticle are displayed in purple. For membrane, the beads of head groups are in blue, and tail beads are in yellow. And the interaction strength (α) is set to 1.3.

The endocytic pathway of spherical particle with a volume of $288\pi\sigma^3$ ($\alpha = 1.6$)

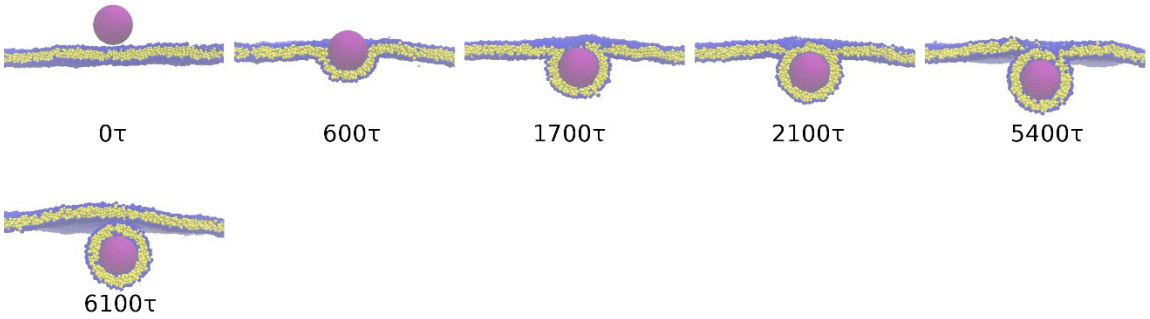

Figure S14: Representative snapshots of endocytic pathway for spherical nanoparticles with a volume of $288\pi\sigma^3$. The interaction strength (α) is set to 1.6.

The endocytic pathway of oblate particle with a volume of $288\pi\sigma^3$ ($\alpha = 1.6$, ρ = 0.4)

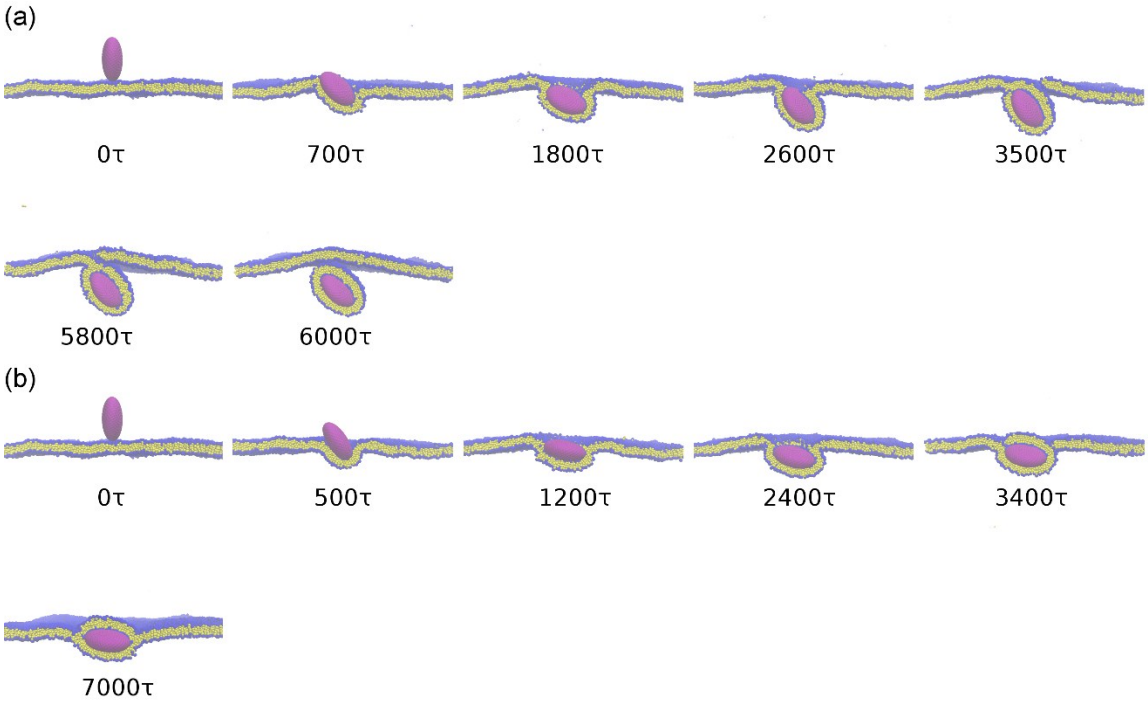

Figure S15: Representative snapshots of two endocytic pathways for oblate nanoparticles (ρ = 0.4) with a volume of $288\pi\sigma^3$. The interaction strength (α) is set to 1.6.

The endocytic pathway of prolate particle with a volume of $288\pi\sigma^3$ ($\alpha = 1.6$, ρ = 3.0)

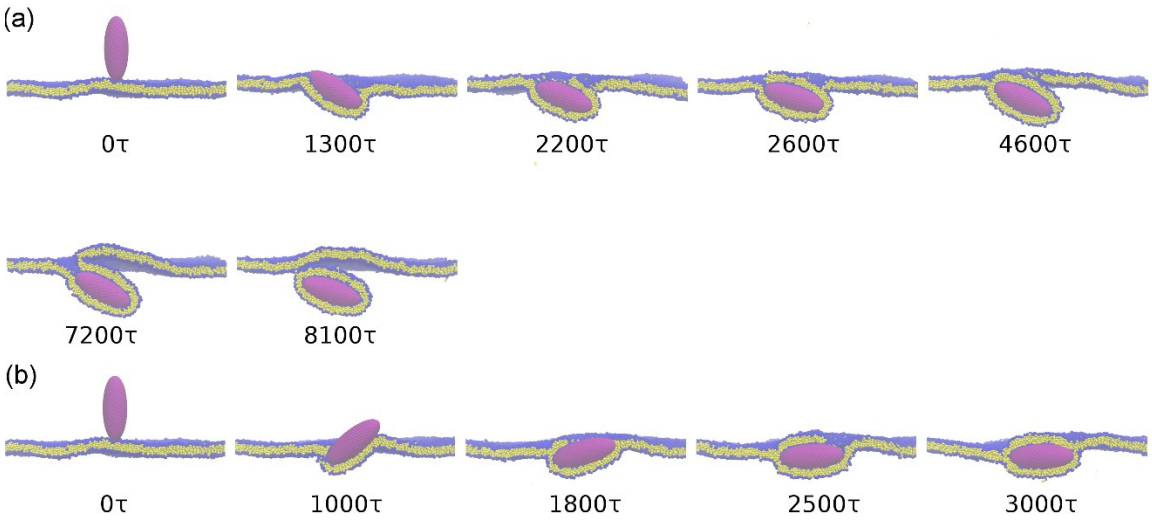

Figure S16: Representative snapshots of two endocytic pathways for prolate nanoparticles (ρ = 3.0) with a volume of $288\pi\sigma^3$. The interaction strength (α) is set to 1.6.

The endocytic pathway of oblate (ρ = 0.4) and prolate (ρ = 3.0) particles with a volume of 972$\pi\sigma^3$ ($\alpha = 1.6$)

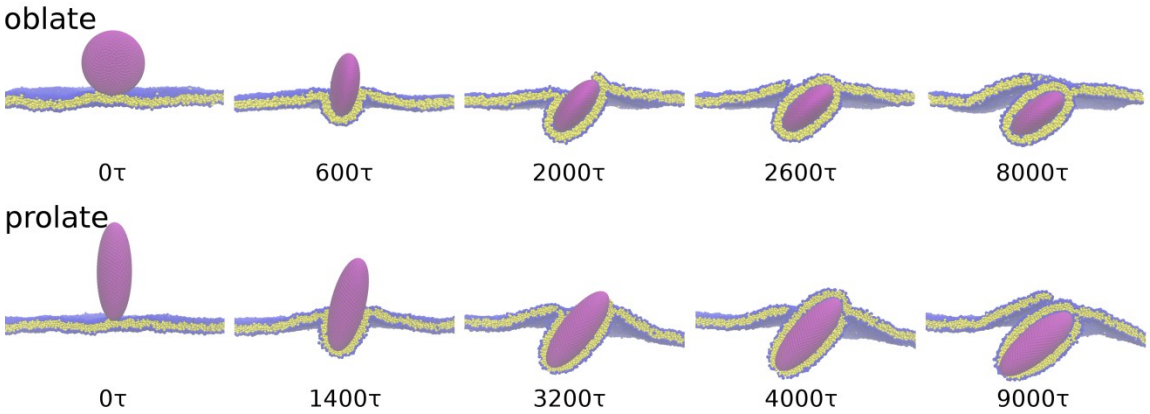

Figure S17: Representative snapshots of endocytic pathways for oblate (ρ = 0.4) and prolate (ρ = 3.0) particles with a volume of $972\pi\sigma^3$. The interaction strength (α) is set to 1.6.

The surface areas of spheroid with different aspect ratios and volume of $288\pi\sigma^3$

The spheroid has two axes with the same length of a, and the third axis with the length of c.

For an oblate spheroid with $c < a$, its surface area can be derived using,

$$S_{oblate} = 2\pi(a^2 + c^2 \frac{\operatorname{arctanh}(\sin\theta)}{\sin\theta}), \quad with\ \theta = \arccos\frac{c}{a} .$$

For a prolate spheroid with $c > a$, its surface area can be derived using,

$$S_{prolate} = 2\pi(a^2 + c^2 \frac{\theta}{\tan\theta}), \quad with\ \theta = \arccos\frac{a}{c} .$$

Here, we list the surface areas of spheroid with a volume of $288\pi\sigma^3$ but varied aspect ratios.

Aspect ratio (ρ)	$a(or\ r = D/2)/\sigma$	Surface area/ $\pi\sigma^2$
0.4	8.143	168.891
0.7	6.757	147.426
1.0	6	144
1.5	5.241	147.922
3.0	4.160	170.179

Table S1 The surface areas of spheroid with a volume of $288\pi\sigma^3$ but different aspect ratios.